Toward accurate tooth segmentation from computed tomography images using a hybrid level set model

Yangzhou Gan
Department of Automation, Shanghai Jiao Tong University, and Key Laboratory of System Control and Information Processing, Ministry of Education of China, Shanghai 200240, China

Zeyang Xia[a)]
Shenzhen Institutes of Advanced Technology, Chinese Academy of Sciences, and The Chinese University of Hong Kong, Shenzhen 518055, China

Jing Xiong[a)]
Shenzhen Institutes of Advanced Technology, Chinese Academy of Sciences, Shenzhen 510855, China

Qunfei Zhao
Department of Automation, Shanghai Jiao Tong University, and Key Laboratory of System Control and Information Processing, Ministry of Education of China, Shanghai 200240, China

Ying Hu
Shenzhen Institutes of Advanced Technology, Chinese Academy of Sciences, and The Chinese University of Hong Kong, Shenzhen 518055, China

Jianwei Zhang
TAMS, Department of Informatics, University of Hamburg, Hamburg 22527, Germany

(Received 11 July 2014; revised 15 October 2014; accepted for publication 27 October 2014; published 11 December 2014)

Purpose: A three-dimensional (3D) model of the teeth provides important information for orthodontic diagnosis and treatment planning. Tooth segmentation is an essential step in generating the 3D digital model from computed tomography (CT) images. The aim of this study is to develop an accurate and efficient tooth segmentation method from CT images.
Methods: The 3D dental CT volumetric images are segmented slice by slice in a two-dimensional (2D) transverse plane. The 2D segmentation is composed of a manual initialization step and an automatic slice by slice segmentation step. In the manual initialization step, the user manually picks a starting slice and selects a seed point for each tooth in this slice. In the automatic slice segmentation step, a developed hybrid level set model is applied to segment tooth contours from each slice. Tooth contour propagation strategy is employed to initialize the level set function automatically. Cone beam CT (CBCT) images of two subjects were used to tune the parameters. Images of 16 additional subjects were used to validate the performance of the method. Volume overlap metrics and surface distance metrics were adopted to assess the segmentation accuracy quantitatively. The volume overlap metrics were volume difference (VD, mm^3) and Dice similarity coefficient (DSC, %). The surface distance metrics were average symmetric surface distance (ASSD, mm), RMS (root mean square) symmetric surface distance (RMSSSD, mm), and maximum symmetric surface distance (MSSD, mm). Computation time was recorded to assess the efficiency. The performance of the proposed method has been compared with two state-of-the-art methods.
Results: For the tested CBCT images, the VD, DSC, ASSD, RMSSSD, and MSSD for the incisor were 38.16 ± 12.94 mm^3, $88.82 \pm 2.14\%$, 0.29 ± 0.03 mm, 0.32 ± 0.08 mm, and 1.25 ± 0.58 mm, respectively; the VD, DSC, ASSD, RMSSSD, and MSSD for the canine were 49.12 ± 9.33 mm^3, $91.57 \pm 0.82\%$, 0.27 ± 0.02 mm, 0.28 ± 0.03 mm, and 1.06 ± 0.40 mm, respectively; the VD, DSC, ASSD, RMSSSD, and MSSD for the premolar were 37.95 ± 10.13 mm^3, $92.45 \pm 2.29\%$, 0.29 ± 0.06 mm, 0.33 ± 0.10 mm, and 1.28 ± 0.72 mm, respectively; the VD, DSC, ASSD, RMSSSD, and MSSD for the molar were 52.38 ± 17.27 mm^3, $94.12 \pm 1.38\%$, 0.30 ± 0.08 mm, 0.35 ± 0.17 mm, and 1.52 ± 0.75 mm, respectively. The computation time of the proposed method for segmenting CBCT images of one subject was 7.25 ± 0.73 min. Compared with two other methods, the proposed method achieves significant improvement in terms of accuracy.
Conclusions: The presented tooth segmentation method can be used to segment tooth contours from CT images accurately and efficiently. [http://dx.doi.org/10.1118/1.4901521]

Key words: image segmentation, level set, tooth, computed tomography, orthodontics

1. INTRODUCTION

Conventionally, orthodontists perform diagnosis and treatment planning by measuring and operating on the dental casts. This process is costly, time-consuming and the accuracy is not satisfactory. In contrast, the individual three-dimensional (3D) digital model of the teeth provides important information to orthodontists for clinical treatments. With the digital model, orthodontists perform diagnosis and treatment planning through manipulating the tooth model in a visualized interface, thereby realizing digital, efficient, and accurate orthodontic treatment.

Laser and gray range images have been broadly used to reconstruct the 3D digital models of the teeth.[1–3] However, these optical images provide only the crown information, while root morphology information, which is necessary for orthodontic treatment, is not included. In contrast, computed tomography (CT) images provide both crown and root information, which makes it possible to reconstruct a complete tooth model. An essential procedure for the tooth model reconstruction from CT images is the tooth segmentation. The tooth segmentation from CT images is a challenging work. First, in the crown part, a tooth may touch its neighbors such that the common boundary between neighboring teeth is missing. Second, in the root part, due to image noise and image intensity similarities between root and surrounding alveolar bone, the root contour may be blurred and the contour extraction is difficult. Third, the tooth contour has flexible topological change and may split into several parts in both crown and root.

There are a few reported automatic or semiautomatic methods for tooth segmentation from CT images. These methods can be categorized into two classes: direct 3D segmentation and two-dimensional (2D) slice by slice segmentation. Methods of the first class extract tooth surface from CT images directly in the 3D volumetric space. Akhoondali *et al.*[4] proposed a fast automatic segmentation method based on region growing algorithm involving four predefined thresholds. As the root and surrounding bone have similar intensities, the region growing and predefined thresholds may fail to distinct them. Keyhaninejad *et al.*[5] and Hosntalab *et al.*[6] proposed to use 2D panoramic image to obtain the tooth bounding box, and then apply a 3D region level set model to extract the tooth surface from the bounding box. The 3D region based level set model used in this method only considered the global intensity statistic to guide the segmentation, and cannot obtain accurate segmentation due to the similarity between the intensity statistic of root and bone. Keustermans *et al.*[7] and Hiew *et al.*[8] developed interactive segmentation methods based on the graph cut algorithm. In these methods, the results of the graph cut are highly dependent on the foreground initialization, and the results may be unrepeatable for different initialization. Methods of the second class extract tooth contours in each 2D slice using tooth contour propagation strategy. Heo and Chae[9] and Wu *et al.*[10] presented to use the intensity prior from the previous slice to estimate the optimal threshold and generate an initial tooth contour, then refine the tooth contour using the B-spline snakes with genetic algorithm. In their methods, the B-spline snakes with genetic algorithm are neither able to separate touching crowns nor deal with the topological changes of the teeth. Gao and Chae[11,12] proposed a level set method with shape and intensity prior to segment tooth from CT images and achieved promising results. This method applied the image gradient with direction detection to guide the tooth contour extraction and adopted the intensity and shape prior to solve the topological change. Yau *et al.*[13] applied the same level set method to extract root contours. Ji *et al.*[14] modified this method to segment anterior teeth (incisor and canine). A major drawback of this method is that "boundary leakage" problem for the root with weak and blurring edge may occur. Additionally, it also suffered from serious accumulated error.

In order to achieve accurate segmentation of tooth from CT images, this paper presents a 2D slice by slice segmentation method based on the level set method. The key contribution of this study mainly includes two aspects. First, a new hybrid level set model which integrates a local binary fitting (LBF) energy, a global intensity prior energy, an edge detection energy, and a shape constraint energy is developed for the segmentation of 2D tooth contours. Second, a mask updating strategy which makes the segmentation of neighboring teeth more flexible is proposed for the separating of touching teeth. To reduce the accumulated errors of slice by slice propagation segmentation, the initialization of the level set function and the shape prior are generated from the results of segmented multiple slices. The proposed method has been validated using 16 sets of cone beam CT (CBCT) images, and the segmentation accuracy and efficiency were assessed quantitatively.

2. METHOD

2.A. Overview

In this paper, it is assumed that the CT images were scanned while subject's teeth were in an open bite position such that no teeth from the maxillary and mandible overlap in one slice. Slices of the maxillary and mandible are segmented independently using the same segmentation procedure. Figure 1 shows the diagram of the segmentation of the maxillary slices. The segmentation procedure contains a user initialization step and an automatic propagation segmentation step. In the user initialization step, the user picks a starting slice and draws a seed point of each tooth in the starting slice. The picked starting slice separates the volumetric images into crown slices and root slices. In the automatic propagation segmentation step, each slice is segmented automatically using the hybrid level set model (described in Sec. 2.B). For the segmentation of the starting slice (see Sec. 2.C), as no prior information is applicable to guide the level set initialization and evolution, the hybrid level set model is extended to a global minimization formulation to extract all possible tooth contours. The extracted contours are then used to recognize those valid tooth contours by incorporating the seed points drawn in the user initialization step. For the segmentation of nonstarting slices, the variational formulation of the hybrid level set model is used. Tooth contour propagation strategy, which propagates the segmented tooth contours of previous slices to the current slice as tooth shape prior, is applied to initialize the

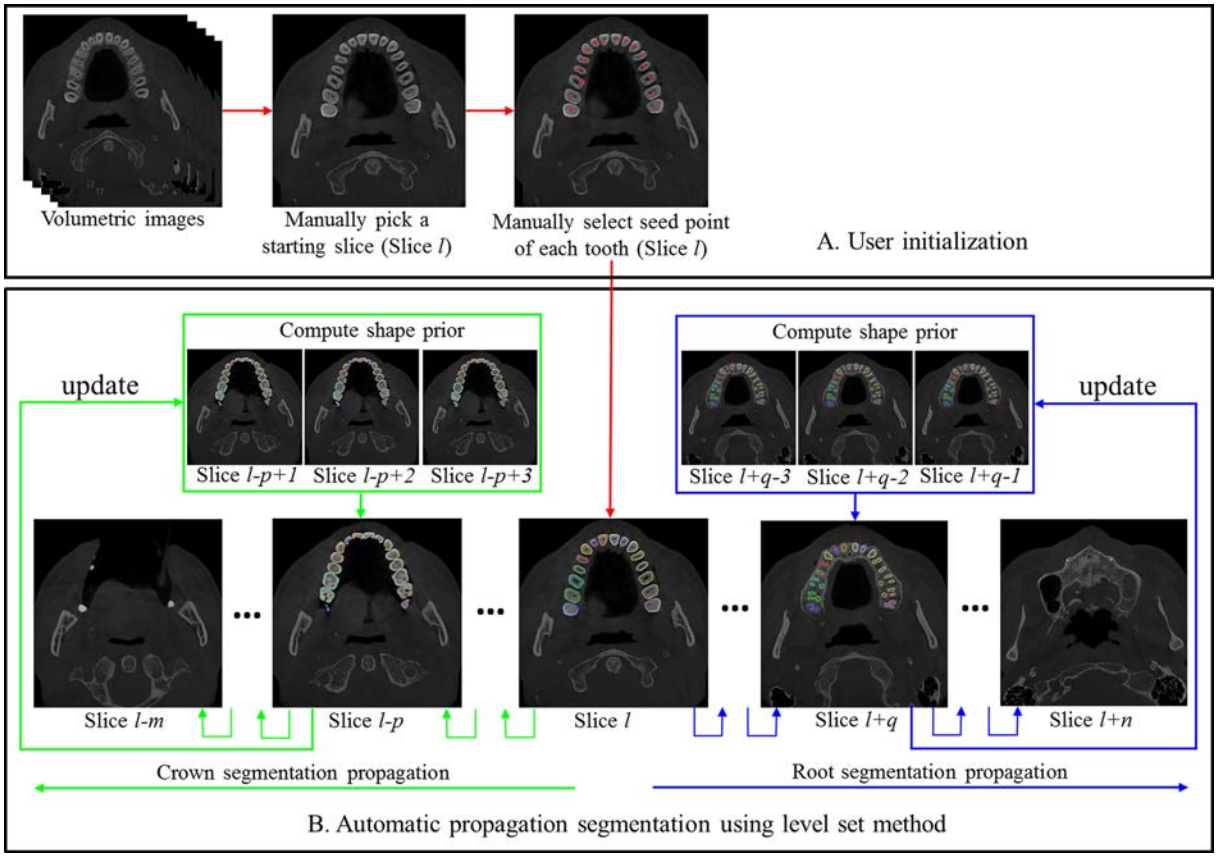

FIG. 1. Diagram of the 2D slice by slice segmentation procedure.

level set function automatically. The propagation proceeds toward the crown and root direction for the crown and root segmentation, respectively, and repeats until no tooth contour is extracted. In order to reduce the accumulated error of the propagation segmentation, tooth shape prior is represented by the average tooth shape of the last three previous segmented slices. The average shape is generated by embedding the tooth shape into the level set function and getting the means of the level set functions. In the case that there are less than three segmented slices, the shape prior is computed from existing segmented slices.

2.B. Hybrid level set model for tooth segmentation

In recent years, the level set method has been increasingly applied to medical image segmentation.[15–18] Conventional level set methods include three types, (I) edge-based models,[19–21] (II) global region-based models,[22,23] and (III) local region-based models.[24,25] Model-I uses the edge information to stop the curve evolution at object boundaries. Generally, it is sensitive to the initial condition and noise, and suffers from serious boundary leakage problems in images with weak edges. Model-II estimates intensities of the foreground and background regions statistically on the total image plane and positions the object boundary according to the global statistical information. Compared to model-I, model-II has many advantages including robustness against initial conditions and insensitivity to image noise. The main limitation of model-II is that it can only separate objects and background with different intensity statistics. When the objects to be segmented have similar intensity statistic with that of the background, model II may fail to segment the objects. Model-III was proposed to segment images with inhomogeneous intensities. Instead of using the global intensity statistic, it utilizes local intensity statistic to realize segmentation of images with weak edge in the presence of inhomogeneous intensities. However, segmentation of model-III relies on the initial condition and may be unstable. For example, when the local region of initial contours does not cover object boundaries, the level set evolves slowly and may get erroneous segmentation.[26,27]

In dental CT images, root and surrounding bones have similar intensities and clear root-bone edge may not exist. In addition, topological change of tooth contour occurs in both root and crown slices. Considering the disadvantages of each single type of the above models, applying only one of them is not able to ensure accurate segmentation. For this purpose, this study develops a hybrid level set model, which incorporates a local intensity energy, a global intensity energy, an edge detection energy, and a shape constraint energy. In the hybrid level set model, the local intensity energy and edge detection energy are applied to guarantee extracting accurate tooth contour in the case that there is no clear tooth edge. The global intensity energy is computed from tooth intensity prior to address the tooth topological change. The prior tooth shape is integrated to constrain the level set evolution toward the prior tooth shape.

2.B.1. Local intensity energy

In this study, Li's LBF model,[24] which has achieved promising results in segmenting object of weak edge with intensity inhomogeneity, is adopted as the local intensity energy. Let Ω be the image plane, I: $\Omega \to \Re$ be a given gray level image, and ϕ: $\Omega \to \Re$ be a level set function on Ω, the energy function of LBF model is defined as

$$\begin{aligned} F(\phi,f_1,f_0) &= \lambda_1 \int_\Omega \left(\int_\Omega K_\sigma(x-y)|I(y)-f_1(x)|^2 H_\varepsilon(\phi(y))dy \right) dx \\ &+ \lambda_2 \int_\Omega \left(\int_\Omega K_\sigma(x-y)|I(y)-f_2(x)|^2 \right. \\ &\left. \times (1-H_\varepsilon(\phi(y)))dy \right) dx + \mu \int_\Omega \delta_\varepsilon(\phi)|\nabla\phi|dx, \end{aligned} \tag{1}$$

where λ_1, λ_2, and μ are positive weights, K_σ is a Gaussian kernel with a scale parameter σ ($\sigma = 2$ in this study), $f_1(x)$ and $f_2(x)$ are the local mean intensities inside and outside the zeros level set, respectively, H_ε is the normalized Heaviside function, and δ_ε is the normalized Dirac delta function.[22]

The first two terms in Eq. (1) are the local intensity fitting energy, and the third term is used to smooth the object contour by penalizing its length. Assuming that the local image intensity is a Gaussian distribution, by applying maximum *a posteriori* probability segmentation, the energy function Eq. (1) can be extended into the following expression:[28,29]

$$\begin{aligned} F(\phi,f_1,f_2,\sigma_1,\sigma_2) &= \int_\Omega \left(\int_\Omega K_\sigma(x-y) \left(\frac{|I(y)-f_1(x)|^2}{2\sigma_1(x)^2} + \log\sigma_1(x) \right) \right. \\ &\left. \times H_\varepsilon(\phi(y))dy \right) dx \\ &+ \int_\Omega \left(\int_\Omega K_\sigma(x-y) \left(\frac{|I(y)-f_2(x)|^2}{2\sigma_2(x)^2} + \log\sigma_2(x) \right) \right. \\ &\left. \times (1-H_\varepsilon(\phi(y)))dy \right) dx + \mu \int_\Omega \delta_\varepsilon(\phi)|\nabla\phi|dx, \end{aligned} \tag{2}$$

where σ_1 and σ_2 are the local standard variances inside and outside the zeros level set, respectively. Compared with Eq. (1), the energy function (2) incorporates the local image variance to guide the segmentation. The coefficients λ_1 and λ_2, which penalize the integrals over inside and outside the zeros level set, respectively, are determined by the standard variances σ_1 and σ_2 adaptively. In fact, the energy function (1) can be considered as a specific case of energy function (2). When the variances of the background and foreground are regarded as constants, the two equations are the same.

In Eq. (2), $f_1(x)$, $f_2(x)$, σ_1, and σ_2 can be derived from the Euler–Lagrange equations of minimizing Eq. (2) for a fixed level set function. And f_1, f_2, σ_1, and σ_2 are written as

$$f_1(x) = \frac{\int_\Omega K_\sigma(x-y)I(y)H_\varepsilon(\phi(y))dy}{\int_\Omega K_\sigma(x-y)H_\varepsilon(\phi(y))dy}, \tag{3}$$

$$f_2(x) = \frac{\int_\Omega K_\sigma(x-y)I(y)(1-H_\varepsilon(\phi(y)))dy}{\int_\Omega K_\sigma(x-y)(1-H_\varepsilon(\phi(y)))dy}, \tag{4}$$

$$\sigma_1(x) = \frac{\int_\Omega K_\sigma(x-y)|I(y)-f_2(y)|^2 H_\varepsilon(\phi(y))dy}{\int_\Omega K_\sigma(x-y)H_\varepsilon(\phi(y))dy}, \tag{5}$$

$$\sigma_2(x) = \frac{\int_\Omega K_\sigma(x-y)|I(y)-f_2(y)|^2(1-H(\phi_\varepsilon(y)))dy}{\int_\Omega K_\sigma(x-y)(1-H(\phi_\varepsilon(y)))dy}. \tag{6}$$

2.B.2. Edge detection energy with direction detection

Gradient is an important information for image segmentation, and has been extensively added into the region-based level set model[30,31] to improve the segmentation. In the hybrid level set model, the gradient information is incorporated through weighting the length penalizing term [the third term in Eqs. (1) and (2)] by an edge indicator g

$$g(x) = \frac{1}{1+|\nabla G_s * I(x)|^2}, \tag{7}$$

where $G_s * I$ is the smoothed version of I by convolving I with the Gaussian kernel G_s, and ∇ denotes the differential operator.

Figure 2(a) shows the tooth construction in the transverse plane. When two neighboring teeth are close enough, two boundaries emerge, and the level set method may fail to distinct the real boundaries of each tooth. In addition, as enamel normally has higher image intensities than dentine, an inner boundary may also emerge. To prevent the zero level set from locating at the neighboring tooth boundaries or the inner boundary, gradient direction detection is needed.[12,32]

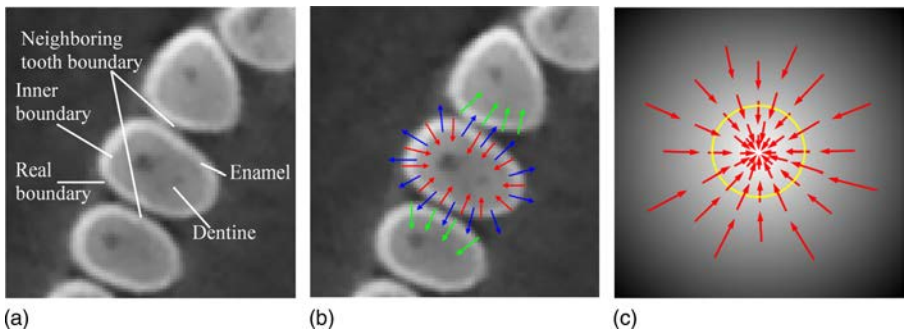

FIG. 2. (a) Tooth construction in the transverse plane. (b) The image gradient directions at the real boundary, inner boundary, and neighboring tooth boundaries. (c) The gradient direction of the level set signed distance function (circular curve denotes the zero level set).

Figure 2(b) indicates the image gradient directions at the real boundary, inner boundary and neighboring tooth boundaries. Figure 2(c) indicates the gradient directions of the level set signed distance function. The image gradients at real tooth boundary point to the inner of the tooth, while the image gradients at the neighboring tooth boundaries or the inner boundary point to the outer of the tooth. The gradients of the level set signed distance function always point to the inner of C. The extracted boundary is the target boundary only when two gradients, the gradient of the image and that of the level set signed distance function, point to the same side. To penalize possible invalid boundary, we use the following edge indicator with gradient direction detection:

$$g(x)=\begin{cases}\dfrac{1}{1+|\nabla G_s * I\phi_0|^2}, & \nabla G_s * I\phi_0 \geq 0\\ 1, & \nabla G_s * I\phi_0 < 0\end{cases} \tag{8}$$

where ϕ_0 denotes the signed distance function to represent the initial tooth contour.

2.B.3. Global intensity prior energy

The tooth intensities between contiguous slices are highly coherent, thus the intensity distribution of the current slice to be segmented should be similar with that of the adjacent slice. In the hybrid level set model, the intensity distribution of the current slice is estimated from the previous segmented slice to define a global region energy.

Let $M=\{M_j|j=f,b\}$ denote the statistical model parameter of either the foreground or background. Assuming that the pixels in each region are independent, based on a maximum *a posteriori* probability segmentation, we can get the following global intensity energy function:

$$F_G(\phi)=\int \log\left(\frac{p(M_b|I(x))}{p(M_f|I(x))}\right)H_\varepsilon(\phi(x))dx, \tag{9}$$

where $p(M_i|I(x))$ is the posterior probability that a given point with intensity $I(x)$ is the foreground or background. The posterior is calculated according to Bayes rule

$$\begin{aligned}p(M_i|I(x))&=\frac{p(I(x)|M_i)p(M_i)}{\sum_{\{i=f,b\}}p(I(x)|M_i)p(M_i)}\\ &\propto p(I(x)|M_i)p(M_i).\end{aligned} \tag{10}$$

Given the foreground and background are *a priori* equally possible, i.e., $p(M_i)=0.5$, the posterior probability $p(M_i|I(x))$ is proportional to the prior conditional probability $p(I(x)|M_i)$. In this study, it is assumed that the image intensity in the local region of the foreground and background is Gaussian distribution. The statistical parameters of Gaussian distribution are estimated from a narrow band (the band width is set to be 5 pixels) around the final zeros level set of the previous slice.

In the dental CT images, the pixel can be categorized into four classes: the tooth, the alveolar bone, the air, and the soft tissues. The air and soft tissues can be separated from the other two tissues using a threshold since the CT values of the air and the soft tissues are always lower than 0 Hounsfield units (HU). The most challenging work in tooth segmentation from CT images is the separation of the tooth from the surrounding alveolar bone due to their similarities of CT values. Thus, in the prior model parameters estimation, only the pixels of the tooth and alveolar bone are used, while the pixels of the air and soft tissues, whose CT value are always less than 0 HU, are not included.

2.B.4. Shape prior constraint energy

Beside the tooth intensities, the tooth shapes between contiguous slices are also highly coherent, and the tooth shape in current slice should change within limited space of the prior tooth shape obtained from the adjacent slices. In this study, the prior tooth shape is represented by the zeros level set implicitly, and incorporated into the hybrid level set model to constrain the level set evolution. The shape constraint energy is defined as the dissimilarity of two shapes represented by their embedding level set functions[33]

$$F_{\text{Shape}}(\phi)=\int (H_\varepsilon(\phi(x))-H_\varepsilon(\phi_0(x)))^2dx, \tag{11}$$

where ϕ_0 denotes the signed distance function of the prior tooth shape. Using Eq. (11) to define the dissimilarity of two shapes, it has the favorable property that the results mainly depend on the sign of the embedded level set function, and one does not need to constrain the level set function to the signed distance function.

The tooth contour has flexible topological change and may split into several branches in both the crown and root. Thus, the level set should have weak shape constraint force inside the zeros level set than that outside the zero level set so that it can split to extract the tooth contour branches. For this purpose, the following expression which adaptively determines the force inside and outside the zero level set of the prior shape is used:

$$F_{\text{Shape}}(\phi)=(1-H_\varepsilon(\phi_0(x)))\int (H_\varepsilon(\phi(x))-H_\varepsilon(\phi_0(x)))^2dx. \tag{12}$$

Thus, the energy function of the developed hybrid level set model is defined as follows:

$$\begin{aligned}F_{\text{hybrid}}(\phi)&=(1-\omega)F_{\text{LBF}}(\phi)+\omega F_G(\phi)+\beta F_{\text{shape}}(\phi)\\ &\quad+\mu\int_\Omega g\delta_\varepsilon(\phi)|\nabla\phi|dx\\ &=(1-\omega)\sum_{i=1,2}\int_\Omega\left(\int_\Omega K_\sigma(x-y)\right.\\ &\quad\times\left.\left(\frac{|I(y)-f_i(x)|^2}{2\sigma_i(x)^2}+\log\sigma_i(x)\right)M_i(\phi)dy\right)dx\\ &\quad+\omega\int\log\left(\frac{p(M_b|I)}{p(M_f|I)}\right)H_\varepsilon(\phi)d+\beta(1-H_\varepsilon(\phi_0))\\ &\quad\times\int(H_\varepsilon(\phi)-H_\varepsilon(\phi_0))^2dx+\mu\int_\Omega g\delta_\varepsilon(\phi)|\nabla\phi|dx,\end{aligned} \tag{13}$$

where ω $(0<\omega<1)$, β, and μ are positive constants, $M_1(\phi)=H_\varepsilon(\phi)$, and $M_2(\phi)=1-H_\varepsilon(\phi)$. The minimization of Eq. (13)

is solved by an explicit iteration scheme based on the following gradient descent flows:

$$\frac{\partial \phi}{\partial t} = \delta_\varepsilon(\phi)\Bigg[(1-\omega)\sum_{i=1,2}(-1)^i \int_\Omega K_\sigma(x-y) \times \left(\frac{|I(y)-f_i(x)|^2}{2\sigma_i(x)^2} + \log\sigma_i(x)\right)dy - \omega\log\left(\frac{p(M_b|I)}{p(M_f|I)}\right) - 2\beta(1-H_\varepsilon(\phi_0)) \times (H_\varepsilon(\phi)-H_\varepsilon(\phi_0)) + \mu\,\mathrm{div}\left(g\frac{\nabla\phi}{|\nabla\phi|}\right)\Bigg], \quad (14)$$

where $t>0$ is the artificial iterative time, div(•) denotes the divergence operator. f_1, f_2, σ_1, and σ_2 are updated before every iteration, and $p(M_b|I)$, $p(M_f|I)$, and g are calculated only once at the beginning of the iteration.

2.B.5. Level set regularization using Gaussian filter

In conventional level set method, a reinitialization procedure is needed to prevent the level set from being too steep or flat. The reinitialization procedure is time consuming. To address the problem, Li *et al.*[24] proposed a regularization term to penalize the deviation of the level set from the signed distance function. As an alternative, this study regularizes the level set after each iteration by convolving the level set function with a Gaussian filter. The Gaussian filter based regularization strategy has been reported to obtain similar results with Li's regularization scheme but is much more efficient.[34]

2.B.6. Stopping criterion

A stopping criterion is important for the level set evolution in guaranteeing computational efficiency and accuracy. Most level set implementations in literature used a fixed maximum number of iterations as the stopping criterion. This may cause unnecessary additional computations or too few iterations to occur. In our numerical implementation, a sign change rate of the level set function is used to detect whether a certain level set converges. When the sign change rate of a certain level set function is lower than a given value [for example, 10exp(-4)] for five consecutive iterations, the iteration of this level set is stopped.

2.B.7. Separation of neighboring teeth

A single level set function can be used to represent any number of objects due to its implicit representation. However, as neighboring teeth touch each other in the crown part, a single level set function may consider the touching teeth as one object and fail to separate them. In order to separate the touching objects, a common solution is to extend the single level set representation to its coupled multiple version, which uses different level sets to represent possible touching objects and introduces a coupled repulsive term to prevent these level sets from crossing each other.[12,31] By applying the coupled multiple version, neighboring teeth can be separated successfully. However, the coupled multiple representation needs level sets evolution over the image plane containing all objects, which results in low efficiency. In contrast, in our implementation, each tooth is represented by an independent level set function. The level set evolution of each tooth is proceeded in a narrow image window containing only the contours of one tooth. To separate neighboring teeth, a mask is used to restrict each level set evolution and preventing from invading into neighboring teeth. The mask is assigned as 0 for points inside the contours of neighboring teeth or 1 for points outside the contours of neighboring teeth [see Fig. 3(b)]. During the segmentation, all level sets are evolved simultaneously, and the mask of each level set is updated before every iteration (as shown in Fig. 4).

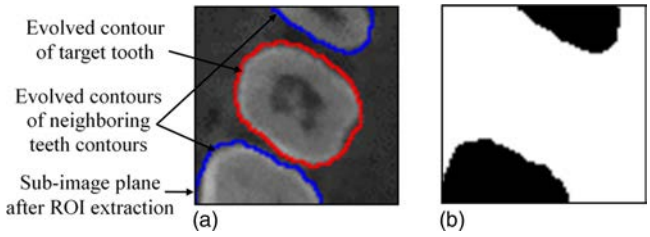

FIG. 3. The mask used for the separation of neighboring teeth. (a) Contours obtained from the previous level set iteration, (b) the mask for the current level set iteration. In the mask, white denotes 1 (the feasible region), black denotes 0 (the infeasible region).

2.C. Segmentation of the starting slice

As introduced in Sec. 2.A, segmentation of the volumetric images starts from picking a starting slice manually and drawing a seed point of each tooth in the starting slice. The starting slice should be picked from the crown slices where all tooth contours are included and no alveolar bone connects with tooth. Figure 5 shows the tooth anatomical structure. It indicates that the crowns of neighboring teeth at the lower part are separate. Picking the starting slice from these slices can facilitate the segmentation of the starting slice.

Neighboring teeth separation algorithm

```
Initialize the p level set functions of HACM;
Given the maximum number of level set iteration n;
for i=2,..., n
    for j=1,..., p
        if stopping criterion is unsatisfied
            calculate the mask m;
            update the j-th level set function: φ_j^i = φ_j^{i-1} + Δφ_j^{i-1}Δt;
            φ_j^i = mφ_j^i;
        end
    end
end
```

FIG. 4. Neighboring teeth separation algorithm using independent level set evolution and mask updating strategy.

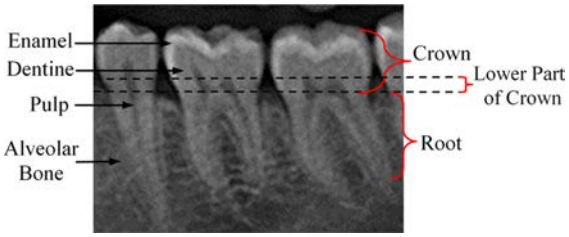

FIG. 5. Tooth anatomical structure.

TABLE I. Parameters configuration for the root segmentation.

Parameters	Incisor	Canine	Premolar	Molar
β	1.0	1.0	1.0	Before splitting: 0.5 After splitting: 1.0
μ	10.0	10.0	10.0	Before splitting: 5.0 After splitting: 10.0

The segmentation procedure of the starting slice is show in Fig. 6. Since no prior intensity and shape can be used, the weight of the global intensity energy and shape constraint energy is set to be zero. Instead of using the variational formulation (14), the global minimization formulation[36] of the hybrid level set model, whose result is independent of initial conditions, is applied to extract all possible tooth regions [Fig. 6(b)]. The seed points drawn in the user initialization step are used to recognize teeth from the extracted regions. Only those regions which cross with the seed points are regarded as valid tooth regions [Fig. 6(c)]. However, it may happen that one region crosses with multiple seed points, which means neighboring teeth are failed to be separated. In this case, a separation line is computed to separate these connected tooth regions[35] [Fig. 6(d)]. For this purpose, the integral intensity values along the center curve of the connected region are used to obtain a profile. The separation point of the separation line corresponds to the local minimum in the profile. The orientation of the separation line corresponds to the perpendicular direction of the center curve of the connected region. More details on the computation of the separation line can be found in Ref. 35.

The global minimization of Eq. (13) (the weights of the global intensity energy and shape constraint energy are set to be zero) can be obtained by minimizing the following energy function:[36]

$$\min_{0\le u\le 1}\int_\Omega g(x)|\nabla u(x)|dx+\frac{1}{\mu}\int_\Omega\sum_{i=1}^{2}(-1)^i\left(\int_\Omega K_\sigma(x-y)\times\left(\frac{|I(y)-f_i(x)|^2}{2\sigma_i(x)^2}+\log\sigma_i(x)\right)u(y)dy\right)dx. \quad (15)$$

Equation (15) is convex and no local minimizer exists. The global minimizer can be solved by carrying out a convex minimization. For the details of the numerical minimization of Eq. (15), please refer to Ref. 37.

2.D. Validation

Totally, CBCT images of 18 subjects were used in this study. Among them, 16 were used to validate the method and other two were used to optimize the parameters of the hybrid level set model [Eq. (14)]. These images were acquired with 120 kV, 5 mA, a matrix of 624×624, a resolution of 0.25 mm isotropic voxel, and the time of exposure of 6 s. All images were scanned while the subjects' teeth were in an open bite position by putting a cotton rod in between to make sure that the lower teeth and the upper teeth do not touch each other. There are no metal artifacts in these images. Before being segmented, the volumetric images have been reoriented manually using the KaVo eXam Vision software (KaVo, Germany) so that the occlusion plane becomes approximately parallel to the transverse plane and most slices in the transverse plane contain all tooth contours. In the hybrid level set model, the parameters were set empirically as $\Delta t = 5.0$ and $\omega = 0.8$. For the crown segmentation, the parameters were also fixed for all teeth as $\beta = 0.5$ and $\mu = 5.0$. For the root segmentation, the optimized parameters were shown in Table I.

Manual segmentation results by experienced clinicians were used as the gold standard to be compared to the algorithm results. To assess the segmentation accuracy quantitatively, five metrics were used. They are the volume overlap metrics: volume difference (VD, mm^3), and Dice similarity coefficient (DSC, %); and the surface distance metrics: average symmetric surface distance (ASSD, mm), RMS (Root mean square) symmetric surface distance (RMSSSD, mm), and maximum symmetric surface distance (MSSD, mm). VD, DSC, and

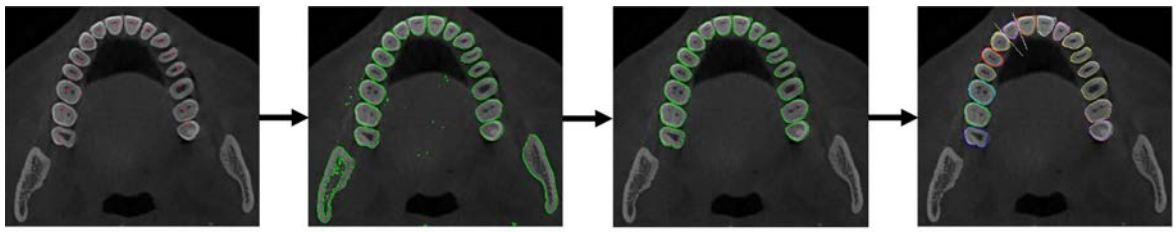

FIG. 6. Diagram of the segmentation of the starting slice. (a) The selected starting slice and the seed points (these marked points). (b) Potential tooth contour extraction using the global minimization formulation of the hybrid level set model. (c) Valid tooth contour recognition based on the seed points in (a). (d) Touching tooth separation by computing the separation line. After the separation of touching teeth, individual tooth contour is obtained.

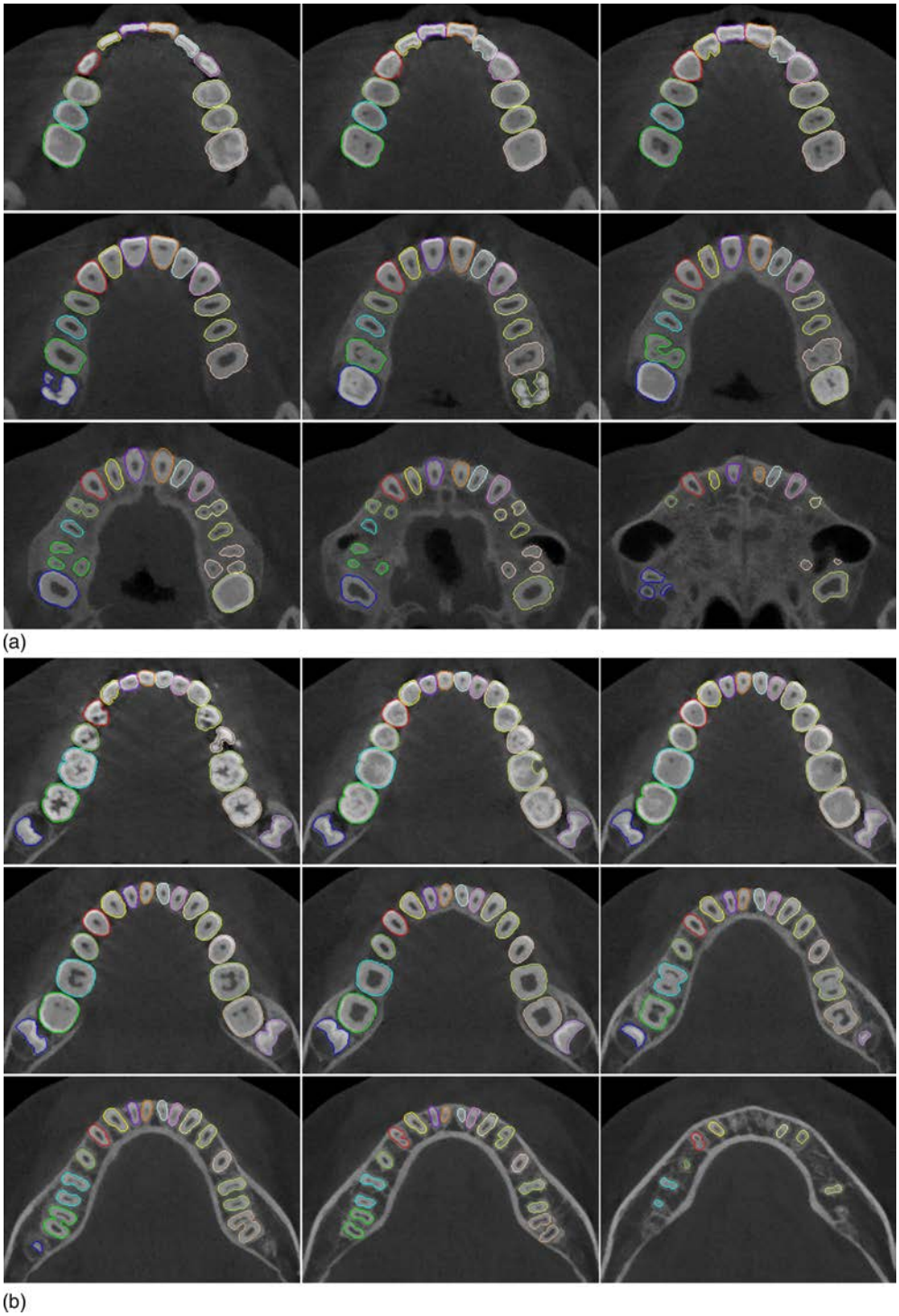

FIG. 7. Segmentation results of the proposed method for the sample slices from one set of volumetric images. (a) Results of the maxillary. (b) Results of the mandible.

ASSD are defined as

$$\mathrm{VD} = |V_R - V_A|, \tag{16}$$

$$\mathrm{DSC} = \frac{2V_R \cap V_A}{V_R + V_A}, \tag{17}$$

$$\begin{aligned}\mathrm{ASSD}(S_R,S_A) = {} & \mathrm{mean}\{\mathrm{mean}\{\mathrm{dist}(a,S_R), a \in S_A\}, \\ & \mathrm{mean}\{\mathrm{dist}(r,S_A), r \in S_R\}\},\end{aligned} \tag{18}$$

where V_R and V_A are the volumes of the gold standard and algorithm segmentation, respectively, S_R and S_A are the surfaces of the gold standard and algorithm segmentation, respectively, $\mathrm{dist}(a, S_R)$ is the nearest Euclidean distance from a surface point a to the surface S_R, and mean $\{\bullet\}$ is the arithmetical average operator. RMSSSD and MSSD are similar to ASSD. Differently, RMSSSD first obtains the squared distances between S_R and S_A, and then extracts the root as the distance.

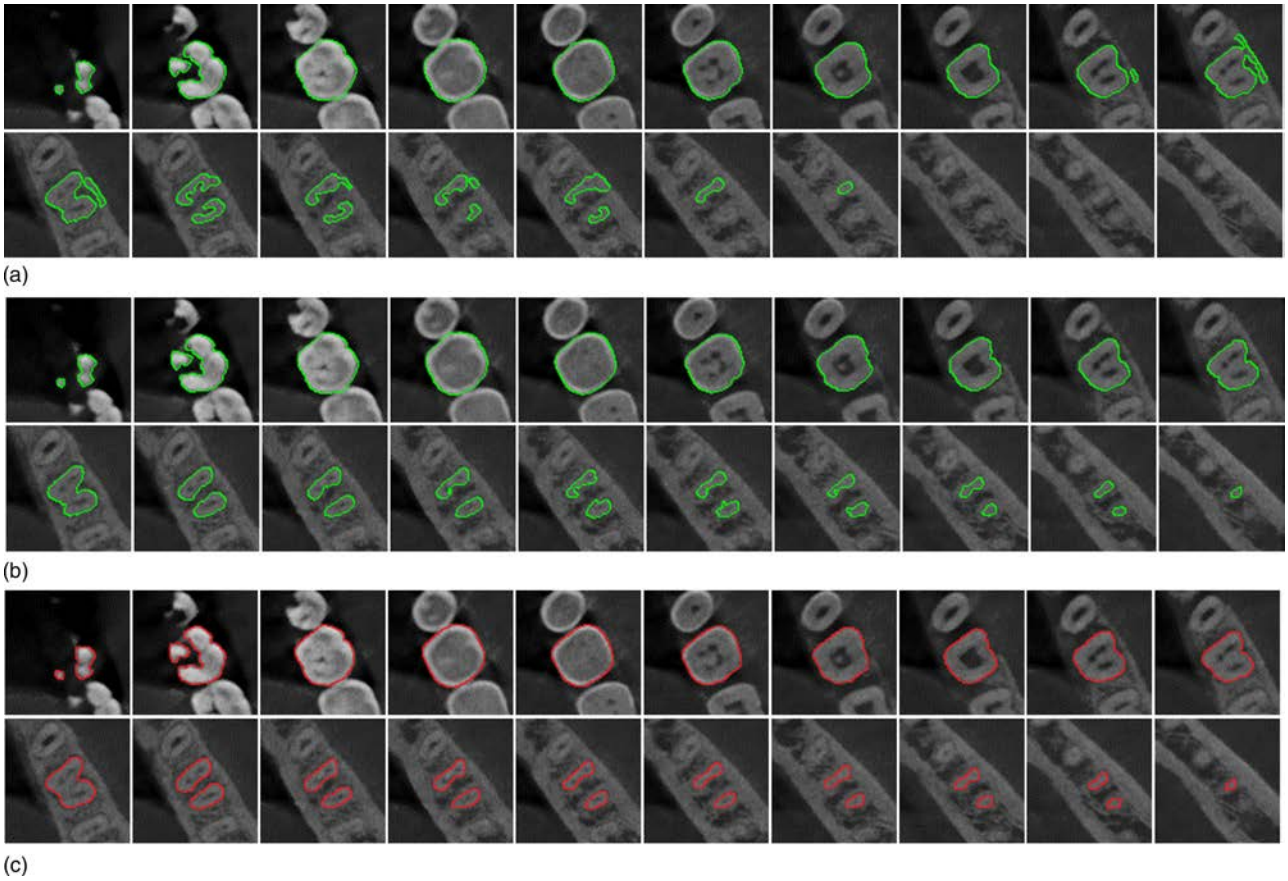

FIG. 8. Qualitative comparison of results of Hosntalab *et al.*'s method to the proposed method for the segmentation of the sample images of a right first mandible molar. (a) The results of Hosntalab *et al.*'s method. (b) The results of the proposed method. (c) The results of the manual segmentation.

While for MSSD, only the maximum of all voxel distances is taken instead of the average.

The presented method was realized using MATLAB code and ran on a DELL graphics workstation (Win 7, Intel E5-2643 3.3 GHz CPU, 16 GB RAM). The processing time for segmenting the tested images was recorded to assess the efficiency of the method.

The intraclass correlation coefficient (ICC) two-way random model on the single measured absolute agreement was used to analyze the reliability of the proposed method. The value of the ICC ranges from 0 to 1, indicating null and perfect reliability, respectively. The reliability is considered as poor, moderate, good, or excellent while ICC ranges 0–0.20, 0.21–0.40, 0.41–0.60, 061–0.80, or 0.81–1.00, respectively.[38] The statistical analysis was performed using SPSS 19.0 software (SPSS, Inc., Chicago, IL).

3. RESULTS

3.A. Qualitative results

Figures 7(a) and 7(b) show the segmentation results of the proposed method for the sample slices of the maxillary and mandible, respectively. The results indicate that the proposed method reconstructs the missing edge between neighboring crowns successfully and obtains individual tooth contours. It also has the ability to segment the roots in the cases that the roots and surrounding bones have similar intensities and the root boundaries are blurring.

The proposed method has been compared to two other state of the art tooth segmentation methods: the Hosntalab *et al.*'s 3D level set based method[6] which belongs to the direct 3D segmentation and the Gao and Chae's level set method with intensity and shape prior[12] which belongs to 2D slice by slice segmentation. Hosntalab *et al.*'s method is an automatic segmentation method which automatically generates the volume of interest (VOI) and initial mask of each tooth using panoramic projection and then applies the 3D level set to extract the tooth surface. However, the automatically generated VOI and initial mask are not always accurate enough for the 3D level set to obtain satisfying tooth segmentation. To be compared fairly, this study applied manually interactive processing to provide VOI and initial mask for Hosntalab *et al.*'s method.

Figure 8 presents the qualitative comparison of the results of Hosntalab *et al.*'s method to the proposed method for a right first mandible molar segmentation. Hosntalab *et al.*'s method segments the tooth from the background based on their global intensity statistic. The intensity statistic in the tooth region is not homogeneous. In addition, the alveolar bone in the background has similar intensity statistic with that of the root. Thus, the global intensity statistic used in

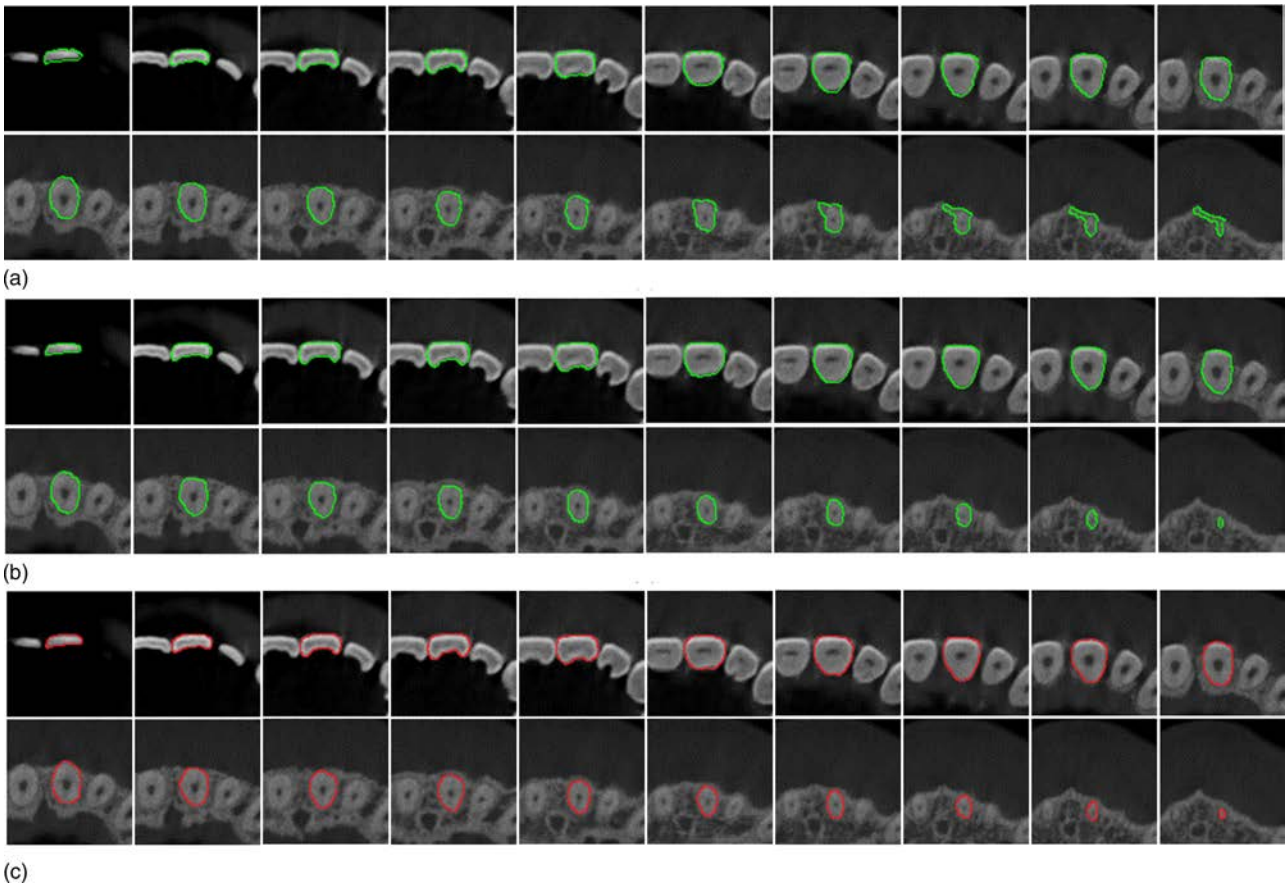

FIG. 9. Qualitative comparison of the results of Gao *et al.*'s method to the proposed method for the segmentation of sample images of a right central maxillary incisor. (a) The results of Gao *et al.*'s method. (b) The results of the proposed method. (c) The results of the manual segmentation.

Hosntalab *et al.*'s method may fail to distinct the tooth from the background. In Fig. 8(a), the extracted tooth contours by this method missed some part of the tooth with relatively low intensities and invaded into the adjacent alveolar bone. While the proposed method obtained the similar results with the manual segmentation.

Figure 9 presents the quantitative comparison of the results of Gao *et al.*'s method to the proposed method for a right central maxillary incisor segmentation. Despite the incorporation of the intensity and shape prior, Gao *et al.*'s method still mainly depends on the image gradient information to guide the segmentation. In the slices where the gradient between the teeth and other bony tissues is not prominent, it is difficult to extract the accurate tooth contours. Figure 9(a) shows that, this method fails to extract the root contours from the surrounding alveolar bone. In addition, the results indicate that this method also suffers from serious accumulated errors. Figure 9(b) shows that the proposed method obtains the similar results with the manual segmentation again.

3.B. Quantitative results

To further estimate the performance of the proposed method, Table II presents the quantitative segmentation accuracy of the proposed method on the tested images for the five metrics: VD, DSC, ASSD, RMSSSD, and MSSD.

Figure 10 presents the quantitative segmentation accuracy of Hosntalab *et al.*'s method, Gao *et al.*'s method, and the proposed method. Compared to Hosntalab *et al.*'s method, for all four types of teeth segmentation, the accuracy improvement of the proposed method in terms of the five metrics is highly significant ($p < 0.01$). Compared to Gao *et al.*'s method, for all

TABLE II. Quantitative segmentation accuracy of the presented method.

	Metrics				
Teeth	VD (mm^3)	DSC (%)	ASSD (mm)	RMSSSD (mm)	MSSD (mm)
Incisor	38.16 ± 12.94	88.82 ± 2.14	0.29 ± 0.03	0.32 ± 0.08	1.25 ± 0.58
Canine	49.12 ± 9.33	91.57 ± 0.82	0.27 ± 0.02	0.28 ± 0.03	1.06 ± 0.40
Premolar	37.95 ± 10.13	92.45 ± 2.29	0.29 ± 0.05	0.33 ± 0.10	1.28 ± 0.72
Molar	52.38 ± 17.27	94.12 ± 1.38	0.3 ± 0.08	0.35 ± 0.17	1.52 ± 0.75

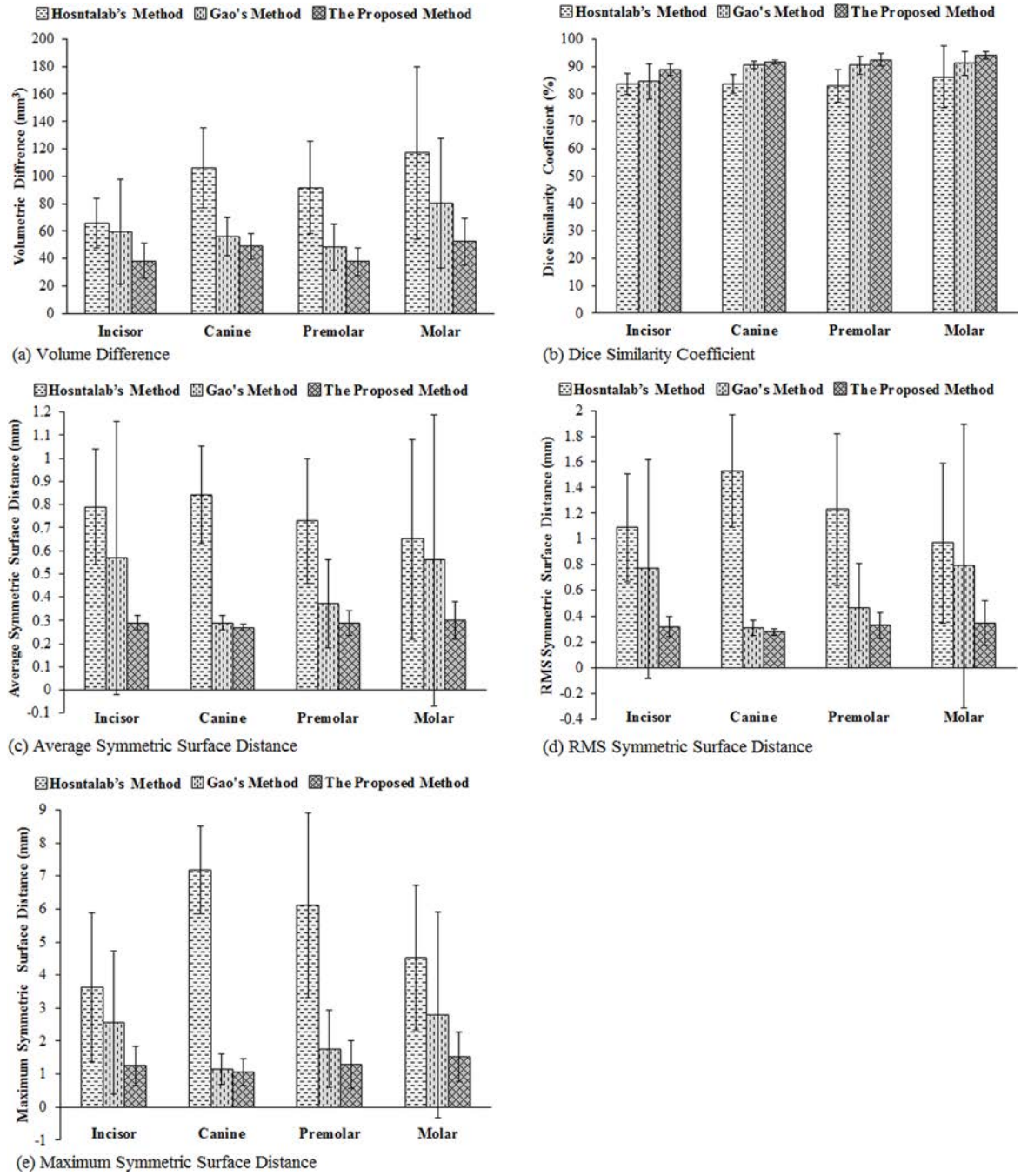

FIG. 10. Quantitative comparison of segmentation accuracy. (a) Volume difference. (b) Dice similarity coefficient. (c) Average symmetric surface distance. (d) RMS symmetric surface distance. (e) Maximum symmetric surface distance.

four types of teeth segmentation, the accuracy improvement of the proposed method in terms of VD and DSC is highly significant ($p < 0.01$), and the improvement in terms of ASSD, RMSSSD, and MSSD is significant ($p < 0.05$).

In the results presented in Fig. 10, the standard deviations of the surface distance metrics of Hosntalab *et al.*'s method and Gao *et al.*'s method are large. This is caused by the outliers with poor segmentation quality. For Hosntalab *et al.*'s method, the outliers happened as a result of over segmentation or under segmentation. Some extracted tooth surface by this method missed some part of the tooth with relatively low intensities or invaded into the adjacent alveolar bone. For Gao *et al.*'s method, the outlier was mainly caused by under segmentation that failed to distinguish the root from surrounding alveolar bone. These outliers with poor segmentation of both methods mainly occurred in the root tip with small volume. The surface distance metrics are rather sensitive to these outliers, thus the standard deviations of the surface distance metrics of the two methods are large. The volume overlap metrics are insensitive to the errors with small volume, thus the standard deviation of volume overlap metrics of the two methods is not so prominent.

The computation time of the proposed method for segmenting the CBCT images of one subject (with 208 slices

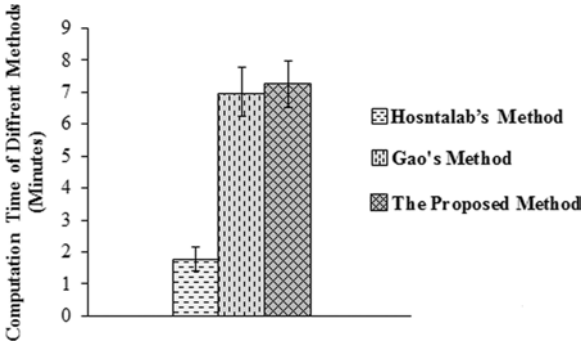

FIG. 11. Computation time comparison of different methods for segmenting CBCT images of one subject.

on average) is 7.25 ± 0.73 min. The comparison of computation time of different methods is presented in Fig. 11. In contrast to the automatic segmentation, manual segmentation normally takes more than 2 h.

3.C. Reliability

CBCT volumetric images of five subjects were randomly selected to evaluate the reliability of the proposed method. Each set of volumetric images was segmented five times by the same trained observer using the proposed method for assessing intraobserver variability. The same images were also segmented once by three other trained observers to perform interobserver variability tests. The intra- and interobserver correlation coefficients are listed in Table III. The intraobserver correlation coefficients of the four types of teeth for the five metrics range from 0.910 to 0.999. The interobserver correlation coefficients of the four types of teeth for the five metrics range from 0.935 to 0.999. The excellent ICC values verify that the proposed method has very small variation across different repetitions and different users, thus the segmentation performance is reliable.

4. DISCUSSIONS

The 3D digital model of the teeth is of clinical importance for computer aided diagnosis and treatment planning in orthodontic treatment. Tooth segmentation is an essential issue in reconstructing the 3D model from CT images. This study presents a 2D slice by slice segmentation method to accurately segment tooth contours from CT images. Compared to the direct 3D segmentation methods, the 2D slice by slice segmentation methods have several advantages. The 3D methods generally need major effort to initialize the 3D tooth surface automatically or interactively, while the 2D methods only need to initialize tooth contours of the starting slice, thus is more feasible. Additionally, it is possible for the 2D methods to use the prior tooth intensity and shape from segmented slices as constraint condition to guide the segmentation.

However, the fatal disadvantage of the 2D slice by slice segmentation methods is the possible accumulated error. In this study, two strategies were developed to reduce the accumulated errors. For the segmentation of the starting slice, whose result is crucial for other slices' segmentation, global minimization formulation of the hybrid level set model is applied. As the result of global minimization formulation is robust to the initial condition, the user does not need to assign each tooth contour. For the maxillary, this strategy is always effective since all crowns are far from the alveolar bone. Figure 12 shows the segmentation results of the eight continuous slices of the maxillary which are regarded as the starting slice and segmented by the starting slice segmentation strategy. The results indicate that the selection of the starting slice and seed points can be quite flexible. However, for the mandible, the possible deformed third molar may touch with the alveolar bone in the crown region. In this case, the segmentation strategy will fail to distinct the third molar contour from the alveolar bone, and the user needs to draw a curve to separate them [as shown in Fig. 13(b)]. The second strategy to reduce the accumulated error is to generate the prior shape from the three previous segmented slices as the initial contour and shape constraint of the current slice. This strategy may obtain relatively accurate initial tooth contours even when the segmentation of previous adjacent slice is incorrect.

The proposed method depends on the developed hybrid level set model to accurately segment tooth contours from each slice. The hybrid level set model shares similar ideas with Gao *et al.*'s model, and can be considered as an improvement of Gao *et al.*'s model. In Gao *et al.*'s model, the global intensity statistic is estimated from the whole image region including the air, soft tissue, and alveolar bone. As the alveolar bone has similar intensity with the tooth, the global intensity energy used in Gao *et al.*'s model can only effectively segment air and soft tissue from the bone tissue, and is difficult to distinguish the alveolar bone from the teeth. In the hybrid level set model, the global intensity statistic is estimated from the alveolar bone and tooth region, while the pixels of air and soft tissue are excluded. As a result, the global intensity energy in the hybrid level set model can more effectively distinguish the

TABLE III. Intraclass correlation coefficients of intraobserver and interobservers segmentation.

	Intraobserver correlation coefficients				Interobserver correlation coefficients			
	Incisor	Canine	Premolar	Molar	Incisor	Canine	Premolar	Molar
VD	0.975	0.981	0.910	0.992	0.954	0.968	0.961	0.995
DSC	0.972	0.962	0.963	0.966	0.935	0.936	0.986	0.966
ASSD	0.998	0.992	0.997	0.999	0.994	0.994	0.997	0.999
RMSSSD	0.998	0.979	0.999	0.999	0.995	0.968	0.999	0.999
MSSD	0.994	0.978	0.997	0.997	0.993	0.977	0.997	0.996

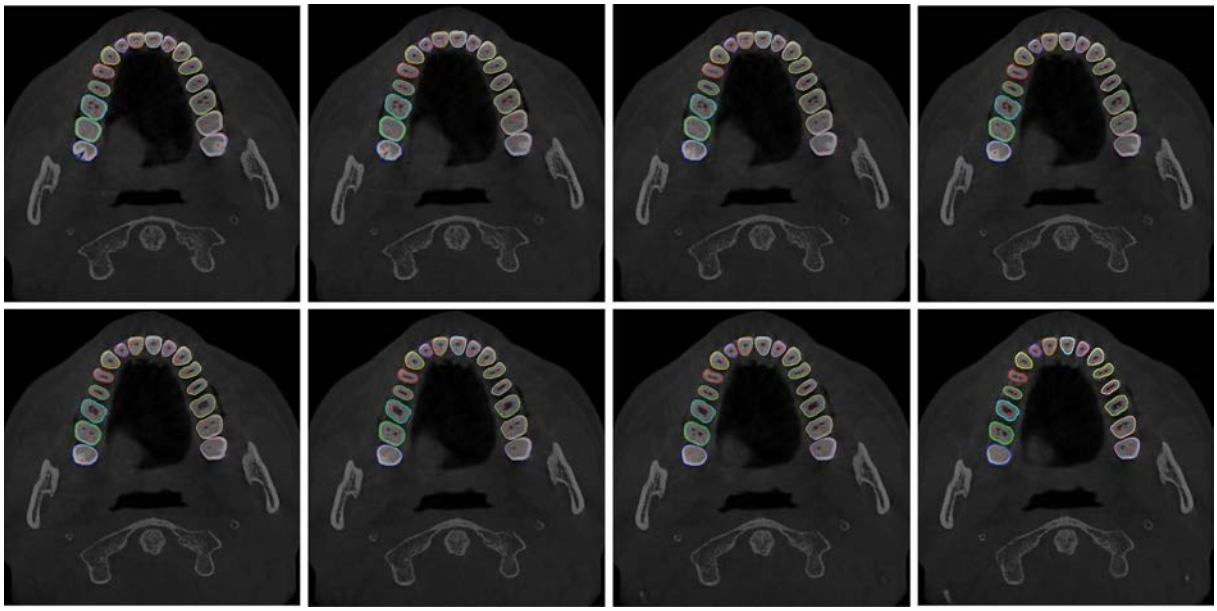

FIG. 12. Segmentation results of continuous slices in the maxillary. These slices are picked as starting slices and segmented by the starting slice segmentation strategy. The red points in these slices denote the picked seed points of each tooth.

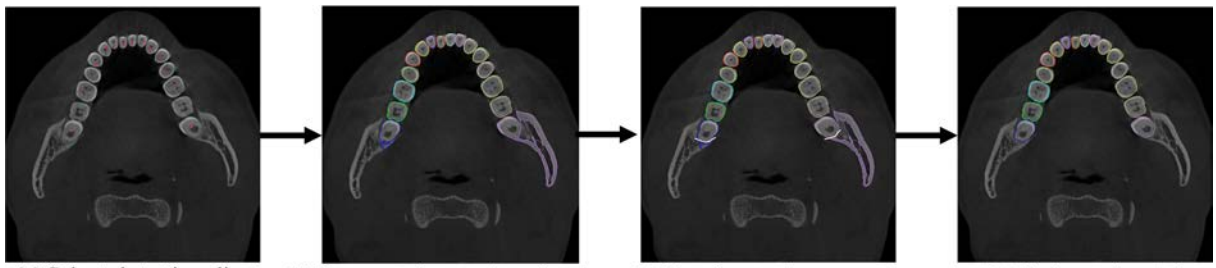

FIG. 13. Interactive segmentation of the starting slice of mandible. (a) The selected starting slice and the seed points. (b) The segmentation results of the starting slice using the starting slice segmentation strategy. As the third molars touch the surrounding alveolar bone, the starting slice segmentation strategy fails to separate them. (c) Interactively drawing the tooth contour (the curves in white color) that were segmented incorrectly. (d) The final segmentation results of the starting slice.

alveolar bone from the teeth. However, as the intensity distribution of a tooth is inhomogeneous, using the global intensity energy of the hybrid level set model to segment the teeth from the alveolar bone cannot get well segmentation quality. To address this issue, a local intensity model which has achieved promising results in segmenting objects with inhomogeneous intensities is integrated into the hybrid level set model to refine the segmentation.

The presented method also has some limitations. First, the volumetric images to be segmented need to be scanned while the subjects' teeth were in an open bite position. For the images scanned in a closed bite position, crowns of the mandible and maxillary would cross each other in some slices, and the presented method is unable to extract accurate crown contours. Second, the presented method cannot segment images with metal artifacts, as the metal artifacts severely degrade the image quality and makes some of the tooth contours unrecognizable. Third, the presented method is difficult to segment images of subjects with impacted teeth. The impacted teeth are buried in the bone, and it is hard to pick a starting slice including all teeth crowns. In the future work, we will try to address these limitations.

5. CONCLUSIONS

This study presents a 2D slice by slice segmentation method for the tooth segmentation from CT images based on the level set method. A hybrid level set model is developed to segment tooth contours form each slice. Validation results on cone beam CT images of 16 objects show that, the proposed method can accurately and efficiently segment tooth contours from CT images and achieves significant accuracy improvement ($p < 0.05$) than other two state of the art tooth segmentation methods.

ACKNOWLEDGMENT

This work was supported by Shenzhen High-level Oversea Talent Program (Peacock Plan) (Grant No. KQCX201306281-12914284).

[a]Authors to whom correspondence should be addressed. Electronic mail: zy.xia@siat.ac.cn and jing.xiong@siat.ac.cn; Telephone: +86-755-86392181/2298.

[1]Y. Hirogaki, T. Sohmura, H. Satoh, J. Takahashi, and K. Takada, "Complete 3-D reconstruction of dental cast shape using perceptual grouping," IEEE Trans. Med. Imaging **20**, 1093–1101 (2001).
[2]J. Gao, W. Xu, and J. Geng, "3D shape reconstruction of teeth by shadow speckle correlation method," Opt. Lasers Eng. **44**, 455–465 (2006).
[3]S. Zheng, J. Li, and Q. Sun, "A novel 3D morphing approach for tooth occlusal surface reconstruction," Comput.–Aided Des. **43**, 293–302 (2011).
[4]H. Akhoondali, R. A. Zoroofi, and G. Shirani, "Rapid automatic segmentation and visualization of teeth in CT-scan data," J. Appl. Sci. **9**, 2031–2044 (2009).
[5]Sh. Keyhaninejad, R. A. Zoroofi, S. K. Setarehdan, and Gh. Shirani, "Automated segmentation of teeth in multi-slice CT images," in *Proceedings of the IET International Conference on Visual Information Engineering, VIE 2006* (IET, Bangalore, India, 2006), pp. 339–344.
[6]M. Hosntalab, R. A. Zoroofi, A. A. Tehrani-Fard, and Gh. Shirani, "Segmentation of teeth in CT volumetric dataset by panoramic projection and variational level set," Int. J. Comput. Assist. Radiol. Surg. **3**, 257–265 (2008).
[7]J. Keustermans, D. Vandermeulen, and P. Suetens, "Integrating statistical shape models into a graph cut framework for tooth segmentation," in *Machine Learning in Medical Imaging* (Springer, Nice, France, 2012), pp. 240–247.
[8]L. T. Hiew, S. H. Ong, and K. W. C. Foong, "Tooth segmentation from cone-beam CT using graph cut," in *Proceedings of the Second APSIPA Annual Summit and Conference, ASC 2010* (APSIPA, Biopolis, Singapore, 2010), pp. 272–275.
[9]H. Heo and O. S. Chae, "Segmentation of tooth in CT images for the 3D reconstruction of teeth," Proc. SPIE **5298**, 455–466 (2004).
[10]X. Wu, H. Gao, H. Heo, O. S. Chae, J. Cho, S. Lee, and Y. Lee, "Improved B-spline contour fitting using genetic algorithm for the segmentation of dental computerized tomography image sequences," J. Imaging Sci. Technol. **51**, 328–336 (2007).
[11]H. Gao and O. Chae, "Touching tooth segmentation from CT image sequences using coupled level set method," in *Proceedings of the IET International Conference on Visual Information Engineering, VIE 2008* (IET, Xian, China, 2008), pp. 382–387.
[12]H. Gao and O. Chae, "Individual tooth segmentation from CT images using level set method with shape and intensity prior," Pattern Recognit. **43**, 2406–2417 (2010).
[13]H. Yau, T. Yang, and Y. Chen, "Tooth model reconstruction based upon data fusion for orthodontic treatment simulation," Comput. Biol. Med. **48**, 8–16 (2014).
[14]D. X. Ji, S. H. Ong, and K. W. C. Foong, "A level-set based approach for anterior teeth segmentation in cone beam computed tomography images," Comput. Biol. Med. **50**, 116–128 (2014).
[15]D. Markel, H. Zaidi, and I. El Naqa, "Novel multimodality segmentation using level sets and Jensen–Rényi divergence," Med. Phys. **40**, 121908 (15pp.) (2013).
[16]M. Abdoli, R. A. J. O. Dierckx, and H. Zaidi, "Contourlet-based active contour model for PET image segmentation," Med. Phys. **40**, 082507 (12pp.) (2013).
[17]W. Qiu, J. Yuan, E. Ukwatta, D. Tessier, and A. Fenster, "Three-dimensional prostate segmentation using level set with shape constraint based on rotational slices for 3D end-firing TRUS guided biopsy," Med. Phys. **40**, 072903 (12pp.) (2013).
[18]K. D. Fritscher, M. Peroni, P. Zaffino, M. F. Spadea, R. Schubert, and G. Sharp, "Automatic segmentation of head and neck CT images for radiotherapy treatment planning using multiple atlases, statistical appearance models, and geodesic active contours," Med. Phys. **41**, 051910 (11pp.) (2014).
[19]M. Kass, A. Witkin, and D. Terzopoulos, "Snakes: Active contour models," Int. J. Comput. Vis. **1**, 321–331 (1988).
[20]R. Malladi, J. A. Sethian, and B. C. Vemuri, "Shape modeling with front propagation: A level set approach," IEEE Trans. Pattern Anal. Mach. Intell. **17**, 158–175 (1995).
[21]V. Caselles, R. Kimmel, and G. Sapiro, "Geodesic active contours," Int. J. Comput. Vis. **22**, 61–79 (1997).
[22]T. Chan and L. A. Vese, "Active contours without edge," IEEE Trans. Image Process. **10**, 266–277 (2001).
[23]J. A. Yezzi, A. Tsai, and A. Willsky, "A fully global approach to image segmentation via coupled curve evolution equations," J. Vis. Commun. Image Represent. **13**, 195–216 (2002).
[24]C. Li, C. Kao, J. C. Gore, and Z. Ding, "Minimization of region-scalable fitting energy for image segmentation," IEEE Trans. Image Process. **17**, 1940–1949 (2008).
[25]S. Lankton and A. Tannenbaum, "Localizing region-based active contours," IEEE Trans. Image Process. **17**, 2029–2039 (2008).
[26]L. Wang, C. Li, Q. Sun, D. Xia, and C. Kao, "Active contours driven by local and global intensity fitting energy with application to brain MR image segmentation," Comput. Med. Imaging Graph. **33**, 520–531 (2009).
[27]Y. Gan and Q. Zhao, "An effective defect inspection method for LCD using active contour model," IEEE Trans. Instrum. Meas. **62**, 2438–2445 (2013).
[28]M. Rousson and R. Deriche, "A variational framework for active and adaptative segmentation of vector valued images," in *Proceedings of IEEE Workshop on Motion and Video Computing, WMVC 2002* (IEEE, Orlando, FL, 2002), pp. 52–62.
[29]L. Wang, L. He, A. Mishra, and C. Li, "Active contours driven by local Gaussian distribution fitting energy," Signal Process. **89**, 2435–2447 (2009).
[30]N. Paragios and R. Deriche, "Geodesic active regions: A new framework to deal with frame partition problems in computer vision," J. Vis. Commun. Image Represent. **13**, 249–268 (2002).
[31]A. Dufour, V. Shinin, S. Tajbakhsh, N. Guillén-Aghion, J. Olivo-Marin, and C. Zimmer, "Segmenting and tracking fluorescent cells in dynamic 3-D microscopy with coupled active surfaces," IEEE Trans. Image Process. **14**, 1396–1410 (2005).
[32]H. Chen and A. K. Jain, "Tooth contour extraction for matching dental radiographs," in *Proceedings of the 17th International Conference on Pattern Recognition, ICPR 2004* (IEEE, Cambridge, UK, 2004), pp. 522–525.
[33]T. Chan and W. Zhu, "Level set based shape prior segmentation," in *Proceedings of IEEE Computer Society Conference on Computer Vision and Pattern Recognition, CVPR 2005* (IEEE, San Diego, CA, 2005), pp. 1164–1170.
[34]K. Zhang, H. Song, and L. Zhang, "Active contours driven by local image fitting energy," Pattern Recognit. **43**, 1199–1206 (2010).
[35]H. Gao and O. Chae, "Automatic tooth region separation for dental CT images," in *Proceedings of the Third International Conference on Convergence and Hybrid Information Technology, ICCIT 2008* (IEEE, Busan, Korea, 2008), pp. 897–901.
[36]T. Chan, S. Esedoglu, and M. Nikolova, "Algorithms for finding global minimizes of image segmentation and denoising models," SIAM J. Appl. Math. **66**, 1632–1648 (2006).
[37]X. Bresson, S. Esedoglu, P. Vandergheynst, J. Thiran, and S. Osher, "Fast global minimization of the active contour/snake model," J. Math. Imaging Vis. **28**, 151–167 (2007).
[38]K. McGraw and S. Wong, "Forming inferences about some intraclass correlation coefficients," Psychol. Methods **1**, 30–46 (1996).